https://doi.org/10.5194/egusphere-2026-1210
Preprint. Discussion started: 18 May 2026

Three-Dimensional Geological Modeling based on Dual-Task Stratigraphy-Aware Attention Networks (Geo-SAN v1.0)

Zhenxi Fang [a], Tongyun Zhang [b], Wuyi Cai [b], Yuzheng Shi [b], Syed Yasir Ali Shah [a], Or Aimon Brou Koffi Kablan [a], and Baoyi Zhang [a, *]

[a] Key laboratory of Metallogenic Prediction of Nonferrous Metals and Geological Environment Monitoring (Ministry of Education) / School of Geosciences and Info-Physics, Central South University, Changsha 410083, China;

[b] Geological and Geographic Information Institute of Hunan Province / Geological Big Data Center of Hunan Province, Changsha 410021, China;

*Corresponding author at: zhangbaoyi@csu.edu.cn (B. ZHANG).

Abstract: The current three-dimensional (3D) geological implicit modelling methods are mainly based on interpolation methods, such as Kriging and radial basis functions (RBFs), which struggle to capture the nonlinear characteristics of complex geological structures and are limited in their capacity to integrate multi-source modeling data. To overcome these limitations, we proposed a 3D geological modelling framework, Geo-SAN, which consists of a dual-task stratigraphy-aware attention network. The framework starts with graph neural networks (GNNs) with a multi-scale neighborhood aggregation mechanism which is aimed to identify critical sampled points adjacent to fault planes and aggregate the lithological features. Subsequently, a stratigraphy-aware attention mechanism is introduced to explicitly incorporate similarities in stratigraphic sequence into the framework. A unidirectional stratigraphic scalar field penalty to lithological classification is developed and incorporated into loss functions, thereby denoising lithological classification. Finally, a dual-task prediction head is designed to simultaneously complete lithological classification and scalar field interpolation. Ablation experiment further validates the contributions of the three core components, that is, graph neighborhood aggregation, stratigraphy-aware attention, and dual-task learning. A case study at the Lingnian-Ningping region of Guangxi Zhuang Autonomous Region (GZAR), China, demonstrates that the proposed Geo-SAN framework, with an accuracy of 92.1% in lithological classification and a coefficient of determination (R^2) of 0.96 in predicting the scalar field, outperforms the Hermite RBFs (HRBFs). In summary, the proposed framework is an important innovation of intelligent modelling of intricate geological formations, which is promising in the application of concealed mineral exploration.

https://doi.org/10.5194/egusphere-2026-1210
Preprint. Discussion started: 18 May 2026

Keywords: three-dimensional geological modelling; graph neighborhood aggregation; stratigraphic sequence; dual-task learning; stratigraphy-aware attention network.

1 Introduction

Three-dimensional (3D) geological modelling is the process of creating mathematical representation of geological structures with the help of suitable computer data structures. The result models are the reflections of the geometrical forms, topological relationships, and spatial distributions of physical and chemical properties of geological bodies. This technique is widely used in earth sciences in visualization, statistical analysis, and numerical simulation (Alcalde et al., 2017; Wang et al., 2019; Du et al., 2026).

3D geological geometric modelling can be divided into explicit and implicit techniques. Explicit modelling generally involves a huge amount of human-computer interaction to connect boundary lines and define the 3D surface model of geological bodies (Sprague and De Kemp, 2005; Caumon et al., 2009; Khan et al., 2021; Shah et al., 2024). Implicit modelling treats geological interfaces as iso-surfaces of a scalar field, thereby preserving topological consistency of geological interfaces. The resulting model automatically satisfies geological contact relationships and facilitates consistent handling of faults and stratigraphic interfaces (Hillier et al., 2013; Guo et al., 2020; Zhang et al., 2023a). Implicit methods, under spatial relationship constraints, can control geological structural topological consistency, orientations of geological structures, and influences of interpolation distances (Khan et al., 2023). They can also integrate geophysical inversion data (such as gravity, magnetic, and seismic) to enhance the ability to interpret deep geological structures (Wellmann et al., 2017; Jessell et al., 2022; Giraud et al., 2024). However, implicit modeling methods suffer limitations such as overfitting in sparse data representation, neglecting lithology classification information, and ignoring geological prior knowledge. An important requirement exists to devise efficient data aggregation methods and reflect correlations between lithology and stratigraphy.

The rapid advancement of deep learning technologies has opened new avenues for 3D geological modelling (Reichstein et al., 2019; Bergen et al., 2019). These methods, collectively termed neural network geomodelling (NNG) (Li et al., 2024; Lyu et al., 2024), encompass graph neural networks (GNNs) (Hillier et al., 2021; Chu et al., 2025; Hu et al., 2024), convolutional neural networks (CNNs) (Bi et al., 2022; Zhang et al.,

https://doi.org/10.5194/egusphere-2026-1210
Preprint. Discussion started: 18 May 2026

2024; He et al., 2025; Ren et al., 2025), and multilayer perceptron (MLP) (Hillier et al., 2023; Guo et al., 2024; Chu et al., 2024). Compared to traditional implicit modelling, neural network modelling approaches offer superior speed and efficiency when handling complex geological structures, enabling their automated modelling, while they require high-quality training data for model training. Since geological sampling data exhibits pronounced spatial irregularity and sparsity (Wang et al., 2012; De La Varga et al., 2019; Wang et al., 2022), Gori et al. (2005) introduced the concept of GNNs, which apply neural network operations on graph-structured data. By propagating information through node connectivity patterns, GNNs accommodate irregular neighborhood structures and are therefore capable of capturing complex geological relationships and structural patterns (Zhang et al., 2023b; Peng et al., 2024; Wang et al., 2024; Yin et al., 2026). Spatial discontinuities arising from geological structures, such as faults, intrusions, and unconformities, further challenge modelling efforts, as traditional similarity-based attention mechanisms struggle to capture contact relationships among geological bodies. Consequently, the direct application of generic attention mechanisms leads to substantial inaccuracies, underscoring the need for deeper integration of stratigraphic sequence and lithological similarity of NNG models.

To address the complexity of geological setting, we propose a 3D geological modelling framework utilizing a dual-task stratigraphy-aware attention network (Geo-SAN), including GNN-based neighborhood aggregation, stratigraphy-aware attention mechanism, and a dual-task prediction head that allows integrating lithological classification and scalar field estimation. To start with, the 3D geological space is modeled as a graph by means of the tetrahedral subdivision, where nodes are sampling points and edges are spatial adjacency. Multi-scale features are extracted and propagated using graph attention networks (GAT) and graph sample and aggregate network (GraphSAGE). Secondly, a new stratigraphy-aware attention mechanism is proposed. This mechanism considers similarities of stratigraphic sequence between the query node and the observation point. Finally, a head of the dual-task prediction is used to collaboratively produce discrete lithological classifications and continuous scalar field estimates.

2 Methods

2.1 Geo-SAN Architecture

The workflow of the proposed 3D geological modelling method (Geo-SAN),

https://doi.org/10.5194/egusphere-2026-1210
Preprint. Discussion started: 18 May 2026

based on a dual-task stratigraphy-aware attention network, is illustrated in Figure 1. The workflow comprises five key stages, graph construction, graph neighborhood aggregation, stratigraphy-aware attention, lithology classification and implicit interpolation, and 3D geological model reconstruction. The method begins with extracting features from sampled data using the graph neighborhood aggregation and stratigraphy-aware attention mechanisms. Subsequently, a dual-task prediction head is employed to estimate both continuous scalar field values and discrete lithological categories. Finally, the predicted result is integrated to construct a coherent 3D geological model.

https://doi.org/10.5194/egusphere-2026-1210
Preprint. Discussion started: 18 May 2026

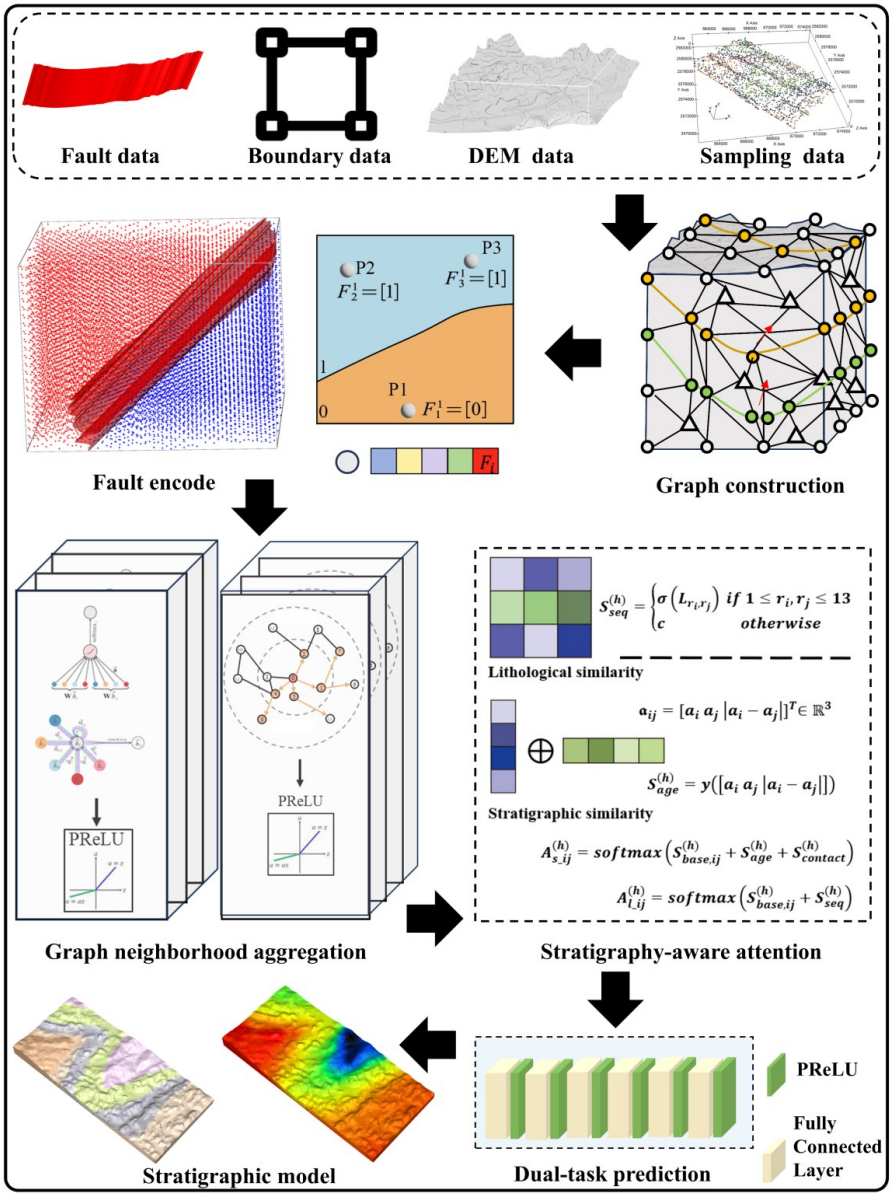

Fig. 1. Workflow of Geo-SAN.

2.1.1 Graph Neighborhood Aggregation

To address the complexity of geological setting and the large volume of geological data inherent in 3D geological modelling, we employ spatial-domain GAT and GraphSAGE to aggregate node features, thereby harnessing the strong nonlinear integration capabilities of GNNs.

https://doi.org/10.5194/egusphere-2026-1210
Preprint. Discussion started: 18 May 2026

(1) Graph Construction

The tetrahedral meshing of the sampled points is performed to create graph structured data. All the sampling points and the other densifying points are both included into the graph data. As shown in Figure 2, the base and the lateral boundaries are determined by the modeling extent whereas the top boundary is determined by the digital elevation model (DEM). Each sampling point is a vertex of a tetrahedron, and the topological connection of the sampling point is maintained during tetrahedron subdivision. Densifying points are created based on the given modelling resolution; overlapping points are eliminated. The resulting mesh has a multi-resolution structure, with tetrahedra around sampled points having smaller volumes and higher densities. Graph nodes are represented as tetrahedral vertices, and graph edges are represented as tetrahedral edges. Finally, the faults are encoded as a feature of nodes in relation to fault planes, which is combined with other node features as model inputs.

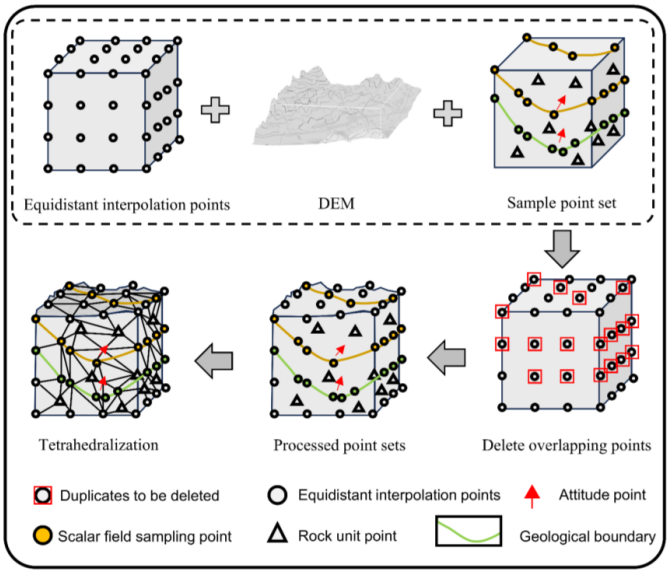

Fig. 2. Graph construction.

(2) GNN Neighborhood Aggregation

The multi-scale graph neighborhood aggregation mechanism is formulated into the proposed framework. GAT with its learnable attention mechanism gives a specific weight to the neighboring nodes (Veličković et al., 2017), which is especially useful in a geological modeling task where local heterogeneity and sensitivity to the boundaries are considered to be a significant issue. When processing nodes near faults, GAT learns

https://doi.org/10.5194/egusphere-2026-1210
Preprint. Discussion started: 18 May 2026

to down-weight connections to neighbors on the opposite side of the fault, effectively preventing spurious propagation of stratigraphic samples across the discontinuity. At stratigraphic boundaries, GAT preferentially attends to aggregate nodes within the same unit, allowing for sharper delineation of geological discontinuities. For node i and its neighbor node j, the attention coefficient α_{ij} is calculated, which reflects the importance of node j in propagating features to node i, as follows:

$$\alpha_{ij} = \frac{\exp\left(\text{LeakyReLU}\left(\boldsymbol{a}^T[\boldsymbol{W}\boldsymbol{h}_i \| \boldsymbol{W}\boldsymbol{h}_j]\right)\right)}{\sum_{k\in\mathcal{N}(i)} \exp\left(\text{LeakyReLU}\left(\boldsymbol{a}^T[\boldsymbol{W}\boldsymbol{h}_i \| \boldsymbol{W}\boldsymbol{h}_k]\right)\right)} \quad (1)$$

where $\boldsymbol{a}$ is the learned attention parameter vector, $\|$ represents the concatenation of feature vectors, $\boldsymbol{W}$ is the weight matrix, and $\boldsymbol{h_i}$ and $\boldsymbol{h_j}$ are the feature representations of nodes i and j, respectively.

GraphSAGE statistically incorporates neighboring node features into the central node through a mechanism primarily designed to capture regional geological characteristics and spatial continuity patterns (Hamilton et al., 2017). For scalar value prediction tasks, this approach demonstrates robust capability in capturing spatial gradient patterns, given that scalar properties within a continuous domain generally exhibit gradational transitions rather than abrupt discontinuities. In lithological classification tasks, GraphSAGE exploits the geological principle that spatially proximate nodes tend to share similar features, thereby incorporating the lithological distribution within the statistical neighborhood to inform classification decisions at each target node. GraphSAGE aggregates the features of neighboring nodes layer by layer through a multi-layer neural network, with the embedding update formula for each layer's nodes, as follows:

$$\boldsymbol{h_v^k} = \sigma\left(\boldsymbol{W^k} \cdot \text{AGGREGATE}_k\left(\left\{\boldsymbol{h_1^{k-1}}, \forall u \in \boldsymbol{N(v)}\right\}\right) \oplus \boldsymbol{h_v^{k-1}}\right)(k = 1, \ldots, K) \quad (2)$$

where $\boldsymbol{h_v^k}$ is the embedding vector of node v at the k layer, $\boldsymbol{N(v)}$ is the neighborhood of node v, and AGGREGATE_k is the aggregation function of the k layer. Common choices for aggregation functions include pooling aggregation and long short-term memory (LSTM) aggregation. Given the similarity of geological features within the same region in geological modeling, the average pooling aggregation function is used in this study to embed the features. $\boldsymbol{W^k}$ represents the learnable weight matrix, and $\oplus$ denotes the vector concatenation operation.

https://doi.org/10.5194/egusphere-2026-1210
Preprint. Discussion started: 18 May 2026

2.1.2 Stratigraphy-Aware Attention Network

Geological data are distinguished by a high degree of spatial heterogeneity, thereby similar characteristics in different geological environments may have entirely distinct meanings. Such domain-specific subtleties are not reflected in conventional attention mechanisms, which only compute weights using feature similarity. To address this weakness, we present a stratigraphy-aware attention (SAN) process that involves the prior constraints of stratigraphic sequences. Through the incorporation of lithological similarity and stratigraphic sequence, the mechanism gains a meaningful combination of stratigraphy knowledge for the proposed framework (Figure 3).

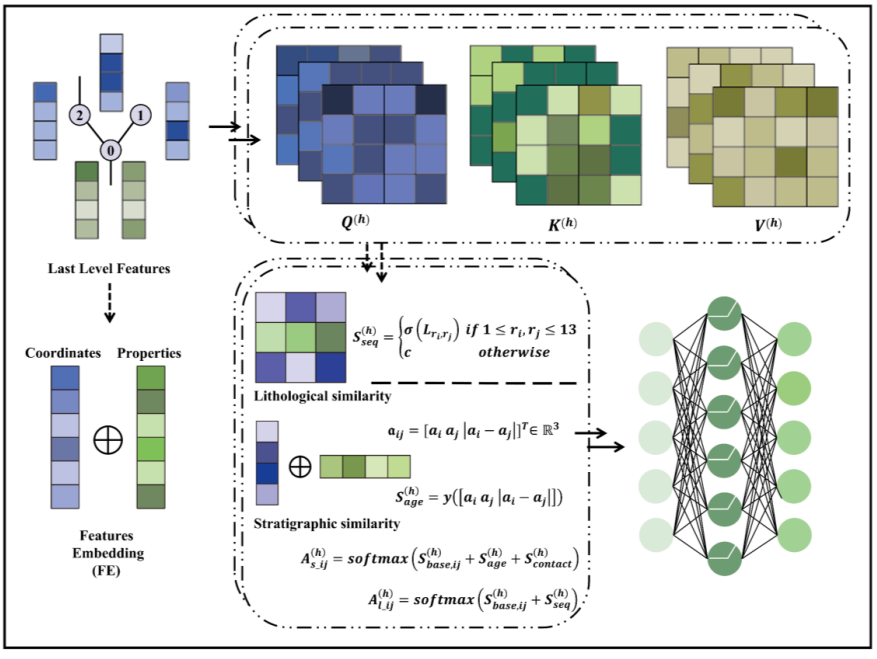

Fig. 3. Stratigraphy-aware attention network.

First, the SAN receives the following inputs: features aggregated from the graph neighborhood, query vectors Q derived from graph nodes, observation point features K from the graph, and feature V used for aggregation. The input features undergo an initial linear transformation that projects them into the attention space. Secondly, the projected features are partitioned into H attention heads, each processing $d_k = d/H$ dimensional features. For nodes i and j, the base score of the h head is:

https://doi.org/10.5194/egusphere-2026-1210
Preprint. Discussion started: 18 May 2026

$$S_{base,ij}^{(h)} = \frac{1}{\sqrt{d_k}} \sum_{l=1}^{d_k} Q_{i,h,l} \cdot K_{j,h,l} \tag{3}$$

We first define the mapping function from lithology to geological age as $a_i = Age(r^i)$, as shown in Figure 4. For node (i,j), the output $S_{age}^{(h)}$ denotes the value for stratigraphic age similarity between node (i,j) at the h head, as follows:

$$S_{age}^{(h)}(i,j) = y\left(\left[a_i\ a_j\ |a_i - a_j|\right]\right) \tag{4}$$

where $y(\cdot)$ is the age mapping function.

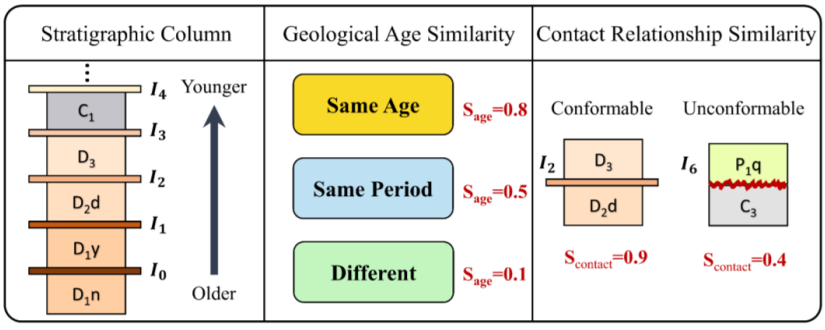

Fig. 4. Stratigraphic similarity

Then, we define a learnable lithological similarity matrix $\boldsymbol{L} \in \mathbb{R}^{K \times K}$, where K is the number of lithological categories. Adjacent strata show stronger lithological similarity, with stratigraphic quantitative difference correlating inversely to lithological resemblance. For nodes i and j, lithological similarity S_{seq} is:

$$S_{seq}^{(h)}(i,j) = \begin{cases} \sigma\left(L_{r_i,r_j}\right) & if\ 1 \le r_i, r_j \le K \\ c & otherwise \end{cases} \tag{5}$$

where $\sigma(x) = \exp(-d(i,j)/3)$, and $d(i,j) = |i-j|$ denotes that the quantitative difference between the ordinal numbers of two lithological categories within the stratigraphic sequence. A lithological similarity matrix from the experiment is shown in Figure 5.

https://doi.org/10.5194/egusphere-2026-1210
Preprint. Discussion started: 18 May 2026

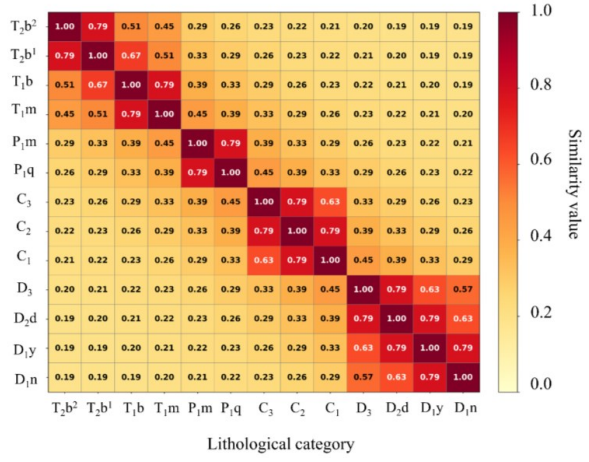

Fig. 5. Lithological similarity matrix.

When predicting scalar values, for the h attention head, the enhancing attention for node pair (i,j) is as follows:

$$A_{s\_ij}^{(h)} = softmax\left(S_{base,ij}^{(h)} + S_{age}^{(h)} + S_{contact}^{(h)}\right) \tag{6}$$

where $S_{contact}^{(h)}$ is the similarity of adjustable contact relationship.

When lithological classification, for the h attention head, the enhancing attention for node pair (i,j) is as follows:

$$A_{l\_ij}^{(h)} = softmax\left(S_{base,ij}^{(h)} + S_{seq}^{(h)}\right) \tag{7}$$

The SAN mechanism begins by computing standard base attention scores through linear projection of node features and their division into multiple attention heads. Its key innovation is the concurrent incorporation of stratigraphic sequence domain knowledge as prior constraints. Specifically, a learnable lithological similarity matrix quantifies the association strength between different lithological categories, while a stratigraphic sequence captures the geological age orders and contact relationship between node pairs. By injecting stratigraphy priors into the attention mechanism, the model allocates weights in a manner that reflects both feature similarity and domain-specific stratigraphic sequences, thereby enabling weighted aggregation and stratigraphic sequence information propagation.

https://doi.org/10.5194/egusphere-2026-1210
Preprint. Discussion started: 18 May 2026

2.1.3 Dual-Task Prediction Module

Following the extraction of spatial perceptual features by the SAN, a dual-task learning head is employed to simultaneously perform lithological classification and scalar field prediction, as illustrated in Figure 6.

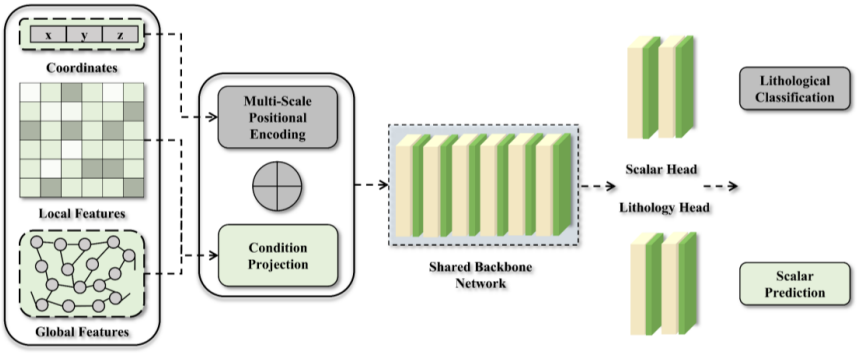

Fig. 6. Dual-task of lithological classification and scalar field prediction.

The dual-task module may consist of two prediction branches which use the same inputs, namely node features with GAT, GraphSAGE, and the SAN mechanism, then the two branches perform distinct tasks by using multilayer perceptron (MLP) decoders. The scalar-field prediction branch produces values of a continuous scalar field [*N*,1], where *N* is number of nodes; the lithological classification branch produces a probability distribution vector [*N*,*K*], where *K*=13 in this study.

2.2 Loss Functions

Three-dimensional geological modeling is a quintessential multi-constrained optimization issue. This study developed the scalar field loss function ($\mathcal{L}_{scalar}$), attitude loss function ($\mathcal{L}_{orientation}$), lithology category loss function ($\mathcal{L}_{litho}$) and stratigraphic constraint loss function ($\mathcal{L}_{strat}$). Figure 7 demonstrates $\mathcal{L}_{scalar}$ measures the discrepancy between the observed scalar value S_v at a sampling point and the predicted scalar value S_v^{scalar} produced by Geo-SAN. The lithological loss $\mathcal{L}_{litho}$ quantifies the disparities between the actual lithological labels and the predicted categories of the model. $\mathcal{L}_{orientation}$ evaluates the discrepancy between the measured direction at orientation sampling points and the direction derived obtained from the predicted scalar field at the corresponding nodes. $\mathcal{L}_{strat}$ converts lithological similarity metrics of stratigraphic sequence into differentiable restrictions, directing neural networks to

https://doi.org/10.5194/egusphere-2026-1210
Preprint. Discussion started: 18 May 2026

acquire predictions aligned with stratigraphy principles. The a priori probability distribution of each lithological categories can be computed and determined according to predicted scalar values. Lithological predictions of the model are then regularized to the prior model with the help of the Kullback-Leibler (KL) divergence penalty, which serves as a soft probabilistic constraint. Meanwhile, a compatibility loss term imposes strict penalties on scalar field predictions falling outside the stratigraphically admissible intervals for corresponding lithological categories. Thus, the cross-task constraint may enforce consistency with stratigraphic sequences to yield geologically meaningful predictions.

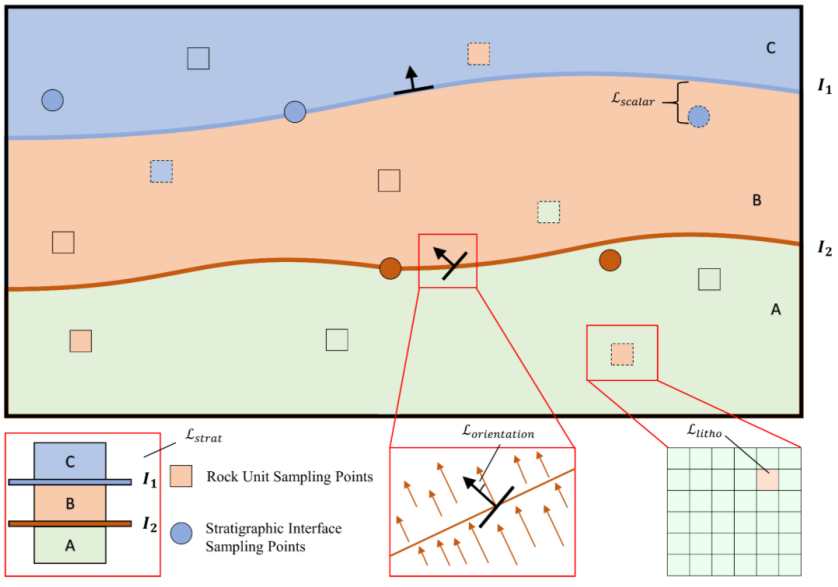

Fig. 7. Loss functions.

2.2.1 Scalar Field Loss Function

Geo-SAN predicts the scalar field f_v, which is constrained by stratigraphic interfaces and orientation points like dip angle and strike. We can define 3D space as a scalar function $f(v)$, where represents the scalar field values at each point v in 3D space. A series of H stratigraphic interfaces can be articulated as:

$$f_1 > \cdots > f_H \tag{8}$$

where f_1 to f_H represent the scalar values of the oldest to newest stratigraphic interfaces, respectively.

For a certain stratigraphic interface I with a scalar field value f_I, the subset of

https://doi.org/10.5194/egusphere-2026-1210
Preprint. Discussion started: 18 May 2026

graph nodes sampled from it can be denoted as:

$$I = \{v \in \boldsymbol{V} | f_v = f_I\} \tag{9}$$

The loss functions $\mathcal{L}_{scalar}$ can be used to find the difference between the scalar field at the stratigraphic interface sampling point and the predicted scalar field by Geo-SAN, as follows:

$$\mathcal{L}_{scalar} = \frac{1}{N}\sum_{i=1}^{N}(\hat{f}_i - f_i)^2 \tag{10}$$

2.2.2 Attitude Loss Function

Nodes with attitudes can be extracted from geological maps, which represent the local morphology of the strata at these nodes. A unit vector $\boldsymbol{n}$ in the normal direction of the stratigraphic interfaces can be transformed from the attitudes:

$$\boldsymbol{n} = \begin{bmatrix} \sin\theta \cdot \sin\delta \\ \cos\theta \cdot \sin\delta \\ \cos\delta \end{bmatrix} \tag{11}$$

where θ and δ are the strike and dip angles of the stratum, respectively.

To measure predicted gradient and the actual direction of angular error, the gradient of the predicted scalar field is gained at these graph nodes. This study employs the first-order Taylor series approximation of the scalar field in the node's first-order neighborhood to estimate the scalar field gradient, as follows:

$$\boldsymbol{P}_v^T \boldsymbol{P}_v \nabla f_v = \boldsymbol{P}_v^T \begin{bmatrix} f_u - f_v \\ \vdots \end{bmatrix} \tag{12}$$

where the angle between the gradient at node v and the known vector $\nabla f_v = (\partial f_v/\partial x, \partial f_v/\partial y, \partial f_v/\partial z)$ can be used to measure the angular error, and u is the neighbor of node v.

$$\boldsymbol{P}_v = \begin{bmatrix} x_u^* - x_v^* & y_u^* - y_v^* & z_u^* - z_v^* \\ \vdots & \vdots & \vdots \end{bmatrix}, \forall\, u \in \boldsymbol{N_v} \tag{13}$$

where x^*, y^*, and z^* are the normalized spatial coordinates of the given node.

The estimated angle between the gradient ∇f_v at node v and the known vector $\boldsymbol{\alpha_v}$ in the observed attitude node-set o is utilized to formulate the loss function, as follows:

$$\mathcal{L}_{orientation} = \sum_{v \in o} \cos(\nabla f_v, \boldsymbol{\alpha_v}) = \sum_{v \in o} \frac{\boldsymbol{\alpha_v} \cdot \nabla f_v}{\|\boldsymbol{\alpha_v}\| \|\nabla f_v\|} \tag{14}$$

2.2.3 Lithology Category Loss Function

In the lithology node-set R, comprising $N_{classes}$ lithology categories, each

https://doi.org/10.5194/egusphere-2026-1210
Preprint. Discussion started: 18 May 2026

lithology node is associated with a one-hot encoded vector $\boldsymbol{l}_v$, denoting its respective lithology category. The loss function employed for lithology nodes is the cross-entropy loss function, as follows:

$$\mathcal{L}_{litho} = -\sum_{v \in R} \left(\boldsymbol{l}_v \cdot \log \left(\hat{\boldsymbol{l}}_v \right) \right) \tag{15}$$

where $\hat{\boldsymbol{l}}_v$ is the predicted probability distribution for node v, and the predicted lithology category is determined based on the highest probability from the softmax distribution of $\hat{\boldsymbol{l}}_v$.

2.2.4 Cross-Task Loss Function

The KL divergence loss function (soft constraint) is utilized to measure the discrepancy between lithological classification and scalar field prediction, thus encouraging models to adhere to stratigraphic sequence patterns, as follows:

$$\mathcal{L}_{KL} = \mathrm{KL}\left(\hat{\boldsymbol{l}} \| \widehat{\boldsymbol{lf}}\right) = \sum_{i=1}^{N} \sum_{j=1}^{K} \hat{\boldsymbol{l}}_i^j \log \frac{\hat{\boldsymbol{l}}_i^j}{\widehat{\boldsymbol{lf}}_i^j} \tag{16}$$

where $\hat{\boldsymbol{l}}_i^j$ denote that model's predicted probability distribution over j-th lithological category at i-th node, and $\widehat{\boldsymbol{lf}}_i^j$ denote that the probability distribution derived from stratigraphic scalar field.

The compatibility loss function evaluates whether expected scalar field conform to the acceptable range for lithological category, imposing penalties on forecasts that contravene geological principles, as follows:

$$\mathcal{L}_{compat} = \frac{1}{N} \sum_{i=1}^{N} \left(1 - \exp\left(-\frac{\Delta f(i)}{F} \right) \right) \tag{17}$$

where F denotes exceeding the upper or lower threshold. The deviation $\Delta f(i)$ measures how far the predicted scalar value is outside the valid range:

$$\Delta f(i) = \max\left(0, \hat{f}_i - tl_i\right) + \max\left(0, bl_i - \hat{f}_i\right) \tag{18}$$

where tl_i and bl_i are the top and bottom interface scalar values according to the observed lithological category at node i. When $bl_i \le \hat{f} \le tl_i$, then $\Delta f(i) = 0$ (perfect compatibility). The cross-task loss function is expressed as:

$$\mathcal{L}_{strat} = \mathcal{L}_{KL} + \mathcal{L}_{compat} \tag{19}$$

The overall loss function is as follows:

$$\mathcal{L} = \alpha \mathcal{L}_{scalar} + \beta \mathcal{L}_{orientation} + \gamma \mathcal{L}_{litho} + \delta \mathcal{L}_{strat} \tag{20}$$

where $\alpha, \beta, \gamma,$ and δ are adjustable parameters.

https://doi.org/10.5194/egusphere-2026-1210
Preprint. Discussion started: 18 May 2026

2.3 Experimental Environment

The experiments in this study are based on the PyTorch Geometric graph machine learning library (Fey and Lenssen, 2019), as shown in Table 1.

Table 1. Experimental environmental.

Configuration	Value
CPU	Intel(R) Xeon(R) Gold 5120 CPU @ 2.20GHz
GPU	NVIDIA GeForce RTX 3090(24G)
Memory (RAM)	128G
Operating system	Ubuntu 24.04.1
Deep learning framework	PyTorch Geometric 2.2.0
CUDA version	12.1

3 Study Area and Dataset

The study area is situated in the Lingnian-Ningping area in Guangxi Zhuang Autonomous Region (GZAR), China (Figure 8). The area predominantly exhibits strata from the Late Paleozoic onwards, therein, strata from the Late Permian (P_3) and Late Triassic to Pleistocene (T_3-N_2) are absent. The Middle Permian (P_2) and Early Triassic (T_1) strata exhibit parallel unconformity, whereas the Middle Triassic (T_2) and Quaternary (Q) strata display angular unconformity. In the central region of the study area, a left-lateral strike-slip reverse fault, the Nacha Fault, intersects the Maokou Formation and Carboniferous strata, dipping southeast at approximately 70° and extending roughly 12 kilometers outside the study area. Within the area, there exist two synclines (I and III) and one anticline (II). Syncline III, located at the center of the study area, has high symmetry, featuring a northeast-trending axial trace, and is truncated along its southern limb by the Nacha Fault. Anticline II is situated in the northwestern section of the study area, demonstrating a notable symmetry and a northeast-oriented axis. Sampling points for stratigraphic interfaces, lithologies, and attitudes were extracted from a planar and four cross-section geological maps (Figure 9) to constitute the modeling dataset. There are 1410 stratigraphic interface sampling points, 18,619 lithology sampling points, and 34 attitude points.

https://doi.org/10.5194/egusphere-2026-1210
Preprint. Discussion started: 18 May 2026

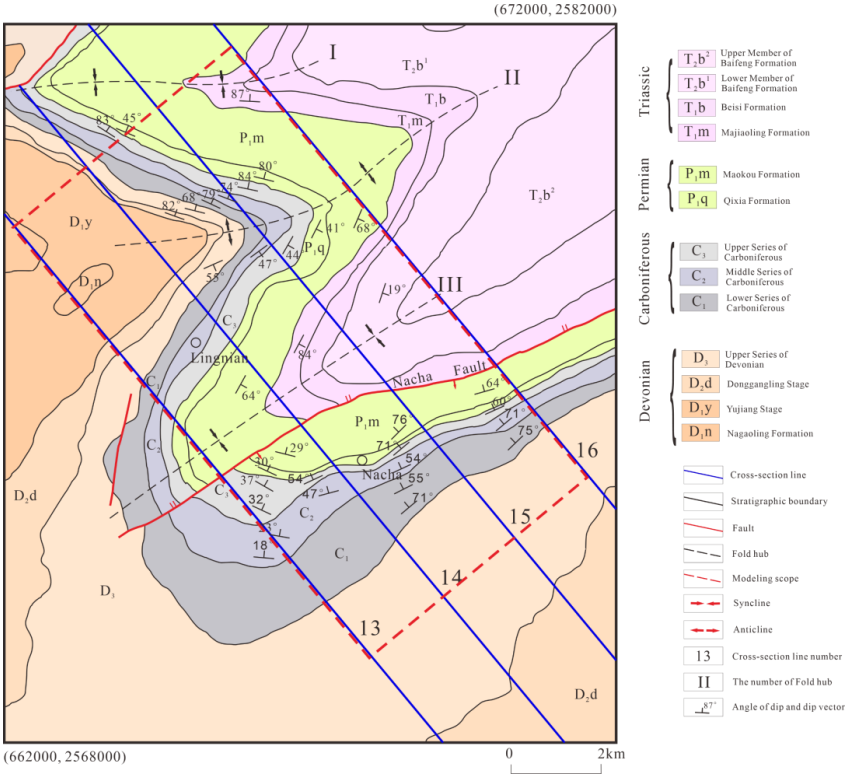

Fig. 8. Geological map of the study area, modified after Zhang et al. (2023a) .

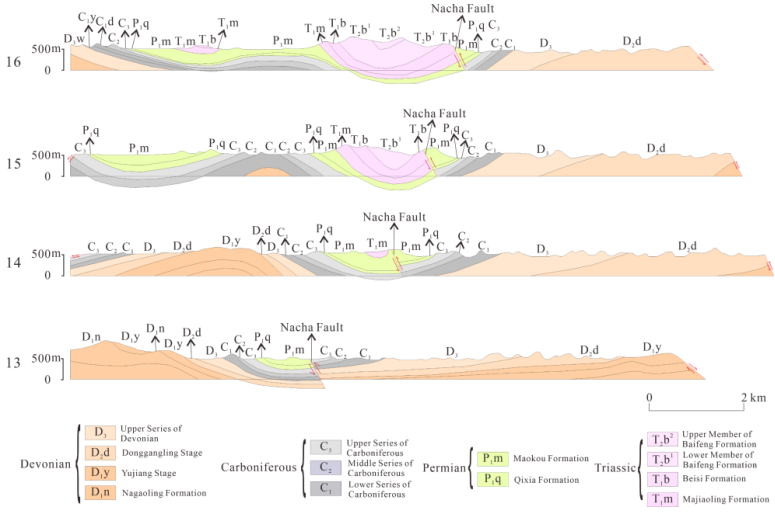

Fig. 9. Geological cross-section maps of the study area, modified after Zhang et al. (2023a).

https://doi.org/10.5194/egusphere-2026-1210
Preprint. Discussion started: 18 May 2026

4 Results

4.1 Model Performance

During model training, various configurations significantly affect performances levels. To evaluate impacts of graph neighborhood aggregation, SAN, and the dual-task learning head modules on overall modeling accuracy, four models were developed, as detailed in Table 2. Model M1 utilizes solely the GAT-based embedding module, while model M2 uses entirely on GraphSAGE for feature embedding. Model M3 employs an alternating technique utilizing both GAT and GraphSAGE embedding while excluding the SAN and the dual-task learning head. Model M4 incorporates three essential modules for comprehensive comparison.

Table 2. Ablation experiments.

Model	Graph neighborhood aggregation	SAN	Dual-task	Description
M1	GAT	√	√	Dual-GAT-SAN
M2	GraphSAGE	√	√	Dual-GraphSAGE-SAN
M3	GAT/GraphSAGE	×	×	GAT-GraphSAGE
M4	GAT/GraphSAGE	√	√	GAT-GraphSAGE-SAN

The ratio of training dataset to testing dataset is set as 8:2, with all models trained according to hyperparameters specified in Table 3.

Table 3. Model hyperparameters.

Hyperparameters \ Model	Graph neighborhood aggregation	Lithology classification /scalar field interpolation
Number of embedding layers	6	8
Learning rate	0.01	0.01
Learning rate scheduler	ReduceLROnPlateau	ReduceLROnPlateau
Learning rate decay	0.8	0.8
Activation function	PreLU	PreLU
Embedding dimension	64	128
Number of attention heads	2	/
Epochs	/	300

To evaluate performances of various models during training, we plot evolution curves for each model over the two tasks: scalar field prediction and lithology classification. Figure 10 illustrates that all four models achieve convergence after

https://doi.org/10.5194/egusphere-2026-1210
Preprint. Discussion started: 18 May 2026

roughly 300 epochs. In the scalar field prediction task, models utilizing the integrated GAT+GraphSAGE embedding exhibit much more quick reductions in loss and root mean square error (RMSE), together with swifter enhancements in the coefficient of determination R^2 (M4 and M3 surpass M1 and M2). This suggests that the GAT+GraphSAGE architecture provides enhanced feature extraction for node-level scalar field interpolation, effectively identifying latent geological patterns during the training process.

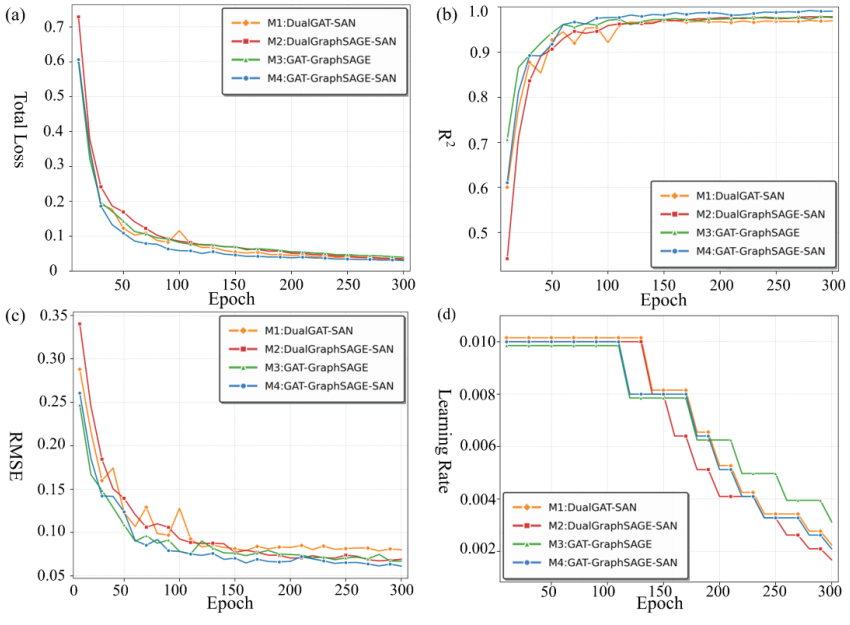

Fig. 10. Model evaluation metrics for scalar field interpolation training processes: (a) total loss, (b) R^2, (c) RMSE, and (d) learning rate.

The lithological classification training curves in Figure 11 show that the SAN-augmented embedding model has a faster decrease in losses and a faster increase in accuracy than the GAT–GraphSAGE model (M3 < M4). This behavior can be explained by the geological principle that lithologies that are close to each other tend to be similar. The SAN effectively directs feature aggregation during training by incorporating lithological similarity and stratigraphic sequence constraints. In contrast, the GAT–GraphSAGE model (M3), which relies solely on graph neighborhood aggregation, lacks the ability to organically integrate stratigraphic sequence prior knowledge during data-driven learning. As a result, its lithological classification performance is noticeably

https://doi.org/10.5194/egusphere-2026-1210
Preprint. Discussion started: 18 May 2026

worse at the beginning of training process.

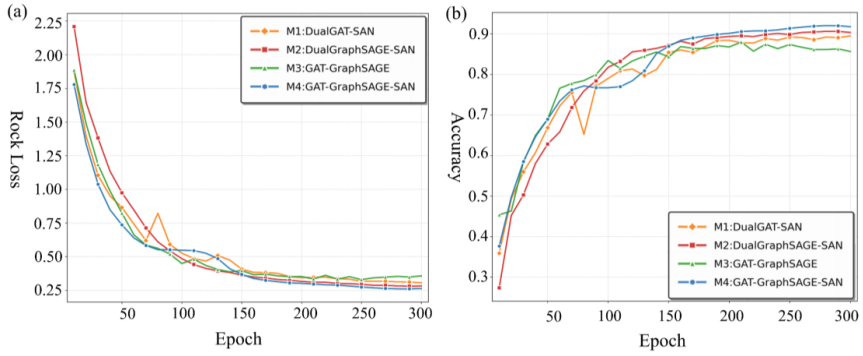

Fig. 11. Model evaluation metrics in lithological classification training processes: (a) loss, and (b) accuracy.

The confusion matrix (Figure 12) shows that the proposed model performs well in all thirteen lithological categories. The model's highest classification accuracy is for D_3 and P_1m lithologies. T_2b^1, C_3, C_1, D_1y, and D_1n have over 85% correctly identified samples, demonstrating strong generalization and stable prediction. Although T_1m and P_1m, and D_2d and D_1y are slightly confused, the overall misclassification remains low, learning meaningful feature representations for each lithological category. Results show three major benefits: (1) Thirteen lithological categories are accurately recognized; (2) Most predictions are correctly along the diagonal with few off-diagonal errors; And (3) residual confusion is between lithologies with similar stratigraphic attributes or transitional relationships. The proposed Geo-SAN model performs well in automated lithology classification under complex geological conditions and provides an intelligent foundation for 3D geological modelling.

https://doi.org/10.5194/egusphere-2026-1210
Preprint. Discussion started: 18 May 2026

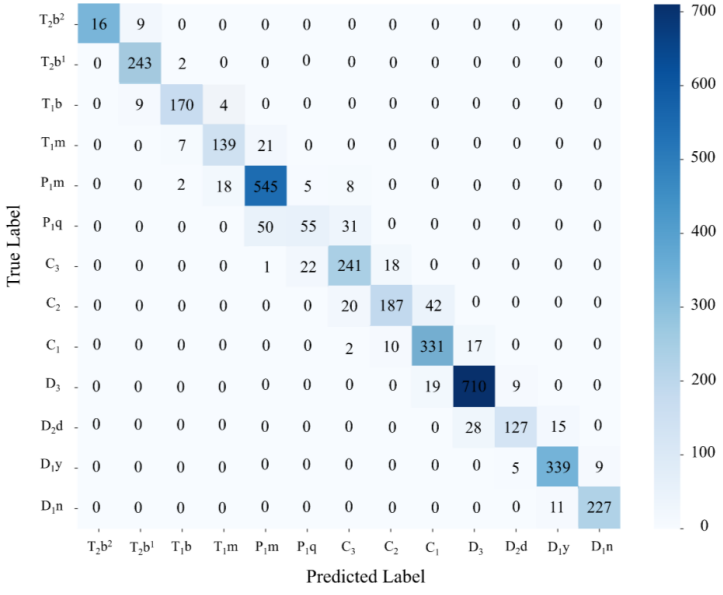

Fig. 12. Geo-SAN lithological classification confusion matrix.

According to category-wise performance metrics (Figure 13), the model demonstrates well in lithological classification. Most lithological categories have F1-scores above 0.80, with T_2b^1, P_1m, D_3, D_1y, and D_1n having values above 0.90, indicating high classification reliability. Most lithology categories, except P_1q (0.671), have precision between 0.79 and 0.99, indicating good false positive control. Most categories maintain recall values between 0.74 and 0.99, indicating high true positive detection rates. The model's robustness under extreme sample imbalance (25 samples of T_2b^2 to 738 samples of D_3) is noteworthy. This shows the Geo-SAN architecture's powerful feature-learning capability and the training strategy's efficacy. Although the recall of P_1q is relatively low (0.404), likely due to its feature similarity with adjacent lithologies, the model still achieves F1-scores above 0.82 for most sparse categories, demonstrating strong small-sample generalization. The model exhibits three major strengths: (1) balanced precision and recall, with most lithological categories achieving values above 0.90 for both metrics; (2) high resilience to sampling imbalance, maintaining stable performance even under severely skewed sample distributions; (3) strong lithological classification applicability, with F1-scores ranging from 0.50 to 0.95.

https://doi.org/10.5194/egusphere-2026-1210
Preprint. Discussion started: 18 May 2026

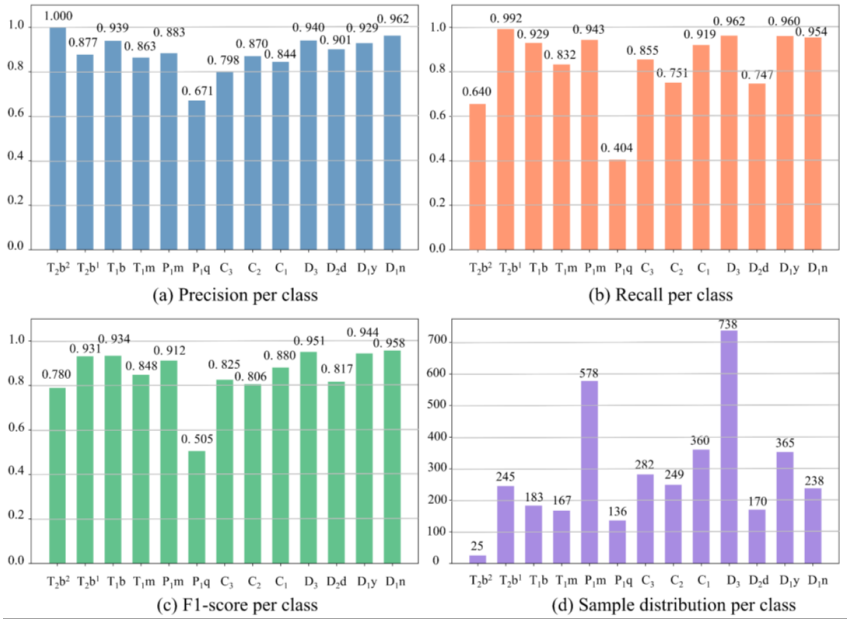

Fig.13. Geo-SAN model lithological classification evaluation metrics.

Further analysis of the model evaluation metrics (Table 4) shows that Model M4 achieves the lowest loss values across its all components after training. This indicates that the integrated strategy, combining GAT+GraphSAGE embedding, SAN, and a dual-task learning head, provides substantially improved predictive performance. For scalar field prediction(evaluated by R^2 and RMSE), the models rank as follows: M4 > M2 > M1 > M3. Models incorporating both GAT and GraphSAGE for scalar field prediction yield higher overall R^2 values and lower RMSEs. For lithology classification (evaluated by accuracy), the performance ranking is: M4 (92%) > M2 (90%) > M1 (90%) > M3 (84%). This demonstrates that GraphSAGE's local feature aggregation, together with the SAN and the dual-task learning structure, significantly enhances lithological classification accuracy.

Table 4. Model performance evaluation metrics (300 epochs).

Model	$\mathcal{L}_{scalar}$	$\mathcal{L}_{orientation}$	$\mathcal{L}_{litho}$	R^2	RMSE	Accuracy	Time
M1	0.0066	0.4735	0.3056	0.95	0.079	0.88	162.15s
M2	0.0049	0.5073	0.2817	0.96	0.070	0.90	127.58s
M3	0.0056	0.5175	0.3956	0.96	0.074	0.84	61.49s
M4	**0.0053**	**0.4541**	**0.2719**	**0.97**	**0.070**	**0.92**	**162.51s**

https://doi.org/10.5194/egusphere-2026-1210
Preprint. Discussion started: 18 May 2026

4.2 Scalar Field

Comparative analysis of scalar fields by Geo-SAN and gradient-adaptive Hermite radial basis function (AdaHRBF) (Zhang et al., 2023a), as shown in Figure 14, shows that both modeling approaches exhibit a broad consistency of large-scale trends and accurately describes the smooth changes of the scalar fields. The AdaHRBF method creates several inharmonious changes in values of scalar fields in structurally complicated areas that are attributed to uneven distribution of sampling points in the spaces and presence of noise which may lead to instability and local distortion. On the other hand, the scalar field generated by Geo-SAN has more gradual and geological smooth transitions in the same areas. The Geo-SAN method improves robustness and local adaptivity by combining SAN and graph-based neighborhood aggregation, creating more robust scalar field representations in complex geological settings.

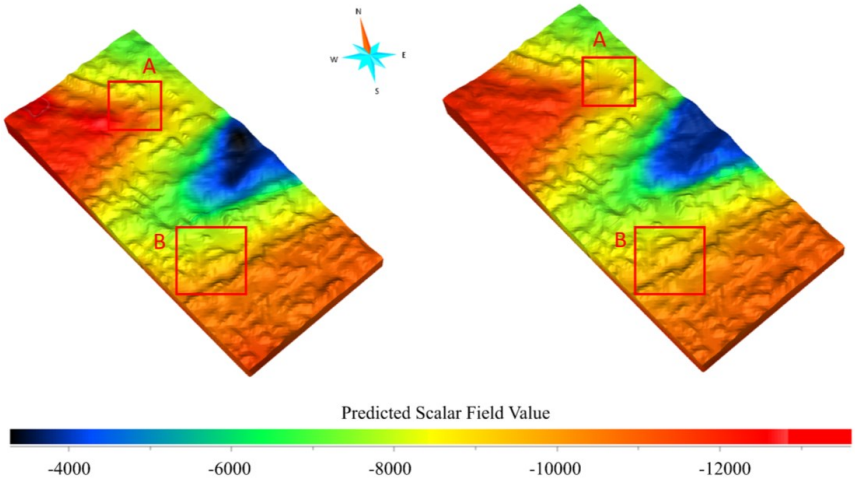

Fig. 14. Three-dimensional scalar fields modeled by (a) AdaHRBF and (b) Geo-SAN.

4.3 Lithology Classification

The proposed Geo-SAN method establishes an inherent coupling between scalar field and lithological categories, thereby enabling direct prediction of lithological classes. In contrast, the AdaHRBF method derives lithological categories indirectly through inequalities of scalar field. Constrained by the DEM surface, two stratigraphic models were reconstructed (Figure 15). Both approaches yield stratigraphic models that reasonably reproduce the major geological structures in the study area, including Synclines I and III and Anticline II. The stratigraphic model generated by the AdaHRBF

https://doi.org/10.5194/egusphere-2026-1210
Preprint. Discussion started: 18 May 2026

method, however, has local unnatural stratigraphic forms(marked in red), and high levels of inconsistency in stratigraphic ordering and thickness distribution on both sides of fault-involved areas. In contrast, the Geo-SAN -based model has good stratigraphic continuity within these structurally complex areas and displays no apparent stratigraphic sequence or thickness anomaly.

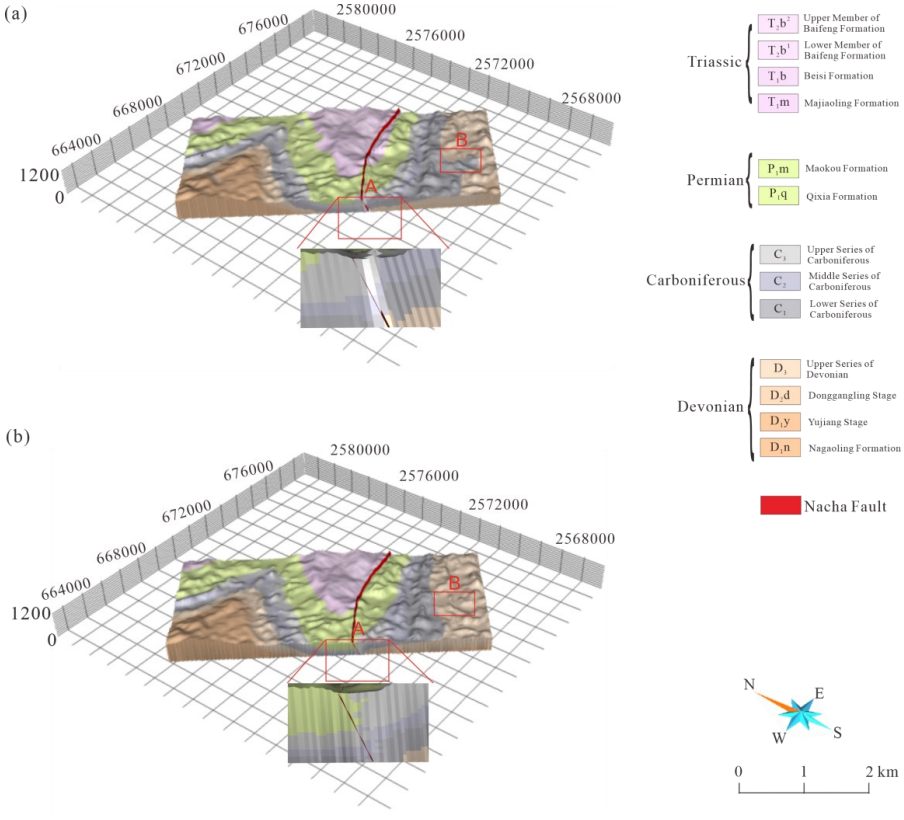

Fig. 15. Three-dimensional stratigraphic models by (a) AdaHRBF and (b) Geo-SAN.

Four geological cross-sections are extracted out of the 3D stratigraphic models by AdaHRBF and Geo-SAN, as shown in Figure 16. Cross-sections gained in the AdaHRBF model indicate unnatural stratigraphic forms that show pronounced inequalities in stratigraphic sequence and changes in thickness on both sides of fault-involved areas. Conversely, the Geo-SAN approach exhibits remarkable stratigraphic consistency in these regions, with no discernible sequence flaws.

https://doi.org/10.5194/egusphere-2026-1210
Preprint. Discussion started: 18 May 2026

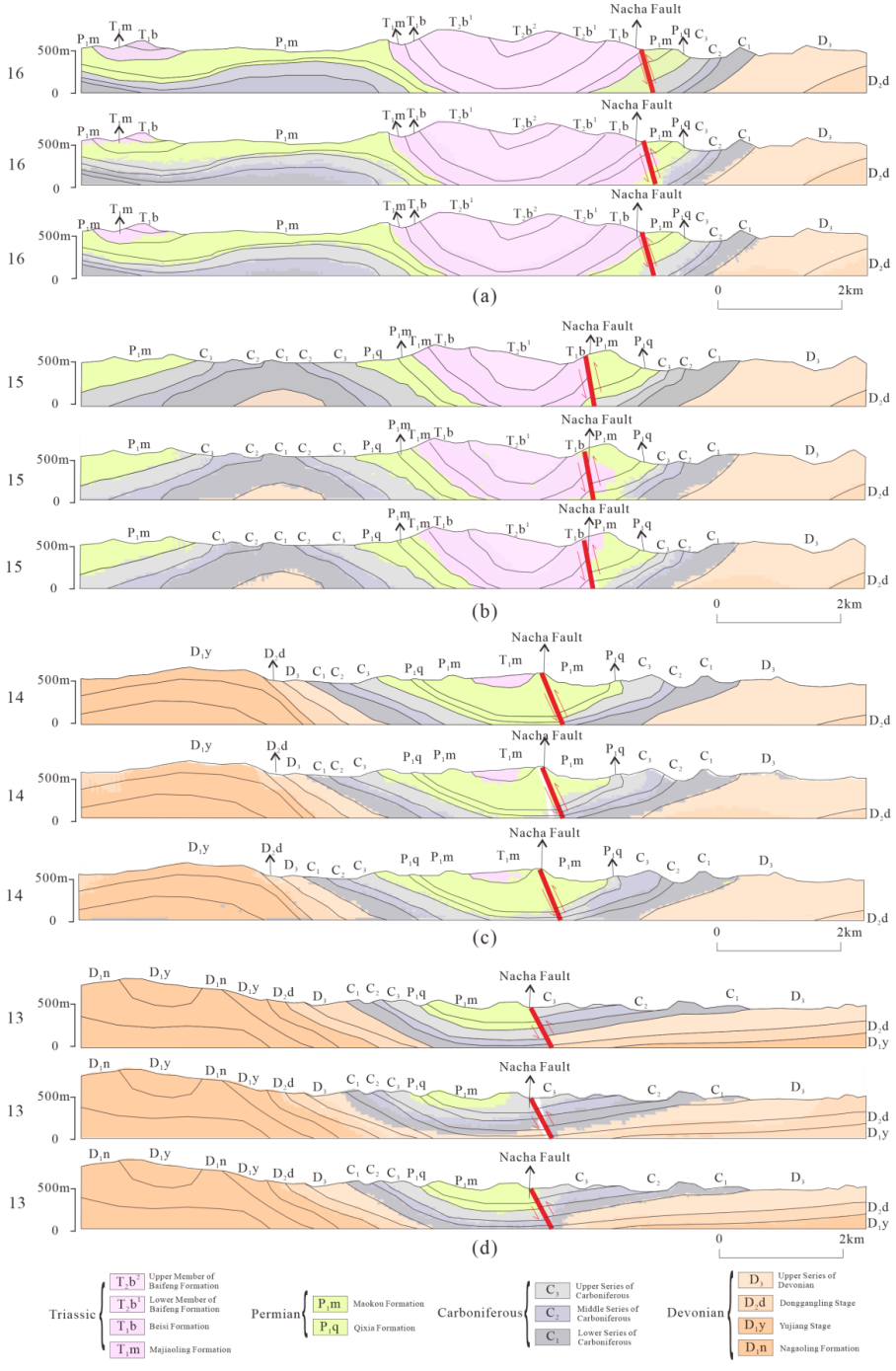

Fig. 16. Compare the cross-section Nos. of (a) 16, (b) 15, (c) 14, and (d) 13 generated by actual, AdaHRBF and Geo-SAN models.

https://doi.org/10.5194/egusphere-2026-1210
Preprint. Discussion started: 18 May 2026

5 Discussions

This study presents a 3D geological modelling framework, Geo-SAN, which is founded upon a dual-task stratigraphy-aware attention network. Unlike conventional implicit modelling methods, which rely on interpolation algorithms and the solution of large-scale linear equations, the suggested method utilizes the message-passing capabilities of GNNs to obtain the multi-scale aggregation of geological data, which is highly effective in overcoming the spatial modelling issues of sparse and irregular sampling points. The scheme is capable of dynamically modifying its feature aggregation strategy based on the lithological similarity and stratigraphic relationship so that a smooth incorporation of data-driven learning and knowledge-driven stratigraphic sequence constraints can be incorporated.

Hillier et al. (2021) used GNNs operating on tetrahedral meshes to perform coupled implicit scalar field modeling and lithological classification. Gao and Wellmann (2025) introduces a fault encoding scheme, in which discontinuous fault data is added as extra binary feature (0/1) to observation and query point positions that allow the neural network to learn to jump the scalar field at faults and to remain continuous elsewhere. The novelty of this paper is based on two main points compared to current deep learning methods: (1) introducing a stratigraphy-aware attention mechanism that incorporates lithological similarity and stratigraphic sequence instead of using pure data-driven fitting to solve the problem, and (2) developing a dual-task framework to establish a cross-task constraints for the link between the scalar field and lithology.

Ablation experiments show that removing the SAN module leads to a 8% decline in classification accuracy, underscoring the essential role of stratigraphical sequence prior knowledge in constraining feature aggregation and improving model robustness. This SAN module applied successfully to 3D geological modelling does not only increase the reliability of the modelling but also offers reference methodology on how to resolve a wide variety of geoscience inverse problems, such as structural reconstruction, geophysical parameter inversion, and subsurface petrophysical property estimation.

Despite these advances, there are still several limitations. First, the framework is still conditional upon training data density and exhibits observable performance regression in case of extremely sparse sampling. Second, the existing framework is highly developed to stratified geological bodies and its applicability to more complex

https://doi.org/10.5194/egusphere-2026-1210
Preprint. Discussion started: 18 May 2026

geological structures, including igneous intrusions, salt domes, and very heterogeneous mixed rocks, has not been confirmed. Third, model interpretability is still limited, and it would be required to conduct more theoretical research on the geological interpretation and internal learning processes of attention weights. Therefore, future improvements are suggested on: (1) active learning to optimize sampling strategy and minimize reliance on the spatial distribution of dataset, (2)adding structural constraint pattern or modeling strategies that use topological relationships to better express irregular boundaries, complicated contact relationships, and spatial topology, and (3) utilizing statistical analysis of attention weight distributions and feature sensitivity analysis to investigate focus of the models under diverse geological settings and their correlation with genuine geological control elements.

6 Conclusions

This study addresses the computational inefficiency, limited capacity for constraint integration, and inadequate treatment of spatial discontinuities commonly encountered by traditional geological implicit modelling methods when dealing with complex geological structures. We introduce a 3D geological modelling framework, Geo-SAN, which consists of a dual-task stratigraphy-aware attention network, and allows the joint optimization of lithological classification and scalar field interpolation. The proposed method obtains a lithological classification accuracy of 92.1% and an R^2 of 0.96 to predict scalar field.

The principal contributions of the study include the following: (1) A multi-scale graph neighborhood aggregation mechanism is developed by alternately integrating GAT and GraphSAGE message-passing layers, which effectively extracts representative features from sparse and irregular sampling data; (2) The stratigraphy-aware attention mechanism is proposed, which uses knowledge of stratigraphic sequence and lithological similarity directly as a part of the feature aggregation mechanism; (3) A dual-task learning architecture is constructed that will complete the task of lithological classification and scalar field prediction simultaneously.

Acknowledgements

This study was supported by grants from the National Natural Science Foundation of China (Grant No. 42572387) and the Scientific Research Project of Geological Bureau of Hunan Province, China (Grant No. HNGSTP202301). We thank Shangguo

https://doi.org/10.5194/egusphere-2026-1210
Preprint. Discussion started: 18 May 2026

Zhou (Institute of Mineral Resources Research, China Metallurgical Geology Bureau) and Xiancheng Mao (Central South University) for their kind assistance with data collection. The authors also thank the MapGIS Laboratory co-constructed by the National Engineering Research Center of Geographic Information System of China and Central South University for providing MapGIS® software (Wuhan Zondy Cyber-Tech Co. Ltd., Wuhan, China).

Code and Data availability

The Geo-SAN v1.0 is available from the GitHub (https://github.com/Geo3D-AI-CSU/Geo-SAN) under the Creative Commons Attribution 4.0 License. The exact version of the model used to produce the results used in this study is archived on Zenodo under DOI: 10.5281/zenodo.19903694 (Fang and Zhang, 2026), as are input data and scripts to run the model and produce the plots for all the simulations presented in this study.

CRediT author statement

ZF: Methodology, Software, and Writing—original draft preparation. **TZ**: Software and Writing—original draft preparation. **WC**: Data curation. **YS**: Investigation and Funding acquisition. **SYAS**: Conceptualization and Writing—review and editing. **OABKK**: Validation and Data curation. **BZ**: Conceptualization, Validation, Writing—review and editing, and Funding acquisition.

Conflict of interest

The authors declared that there is no conflict of interest.

References

Alcalde, J., Bond, C. E., Johnson, G., Butler, R. W., Cooper, M. A., and Ellis, J. F.: The importance of structural model availability on seismic interpretation, Journal of Structural Geology, 97, 161-171, 2017.

Bergen, K. J., Johnson, P. A., de Hoop, M. V., and Beroza, G. C.: Machine learning for data-driven discovery in solid Earth geoscience, Science, 363, eaau0323, 2019.

Bi, Z. F., Wu, X. M., Li, Z. L., Chang, D. K., and Yong, X. S.: DeepISMNet: three-dimensional implicit structural modeling with convolutional neural network, Geosci Model Dev, 15, 6841-6861, 10.5194/gmd-15-6841-2022, 2022.

Caumon, G., Collon-Drouaillet, P., Le Carlier de Veslud, C., Viseur, S., and Sausse, J.: Surface-Based 3D Modeling of Geological Structures, Mathematical Geosciences, 41, 927-945, 10.1007/s11004-

https://doi.org/10.5194/egusphere-2026-1210
Preprint. Discussion started: 18 May 2026

009-9244-2, 2009.
Chu, D., Fu, J., Wan, B., Li, H., Li, L., Fang, F., Li, S., Pan, S., and Zhou, S.: A multi-view ensemble machine learning approach for 3D modeling using geological and geophysical data, International Journal of Geographical Information Science, 38, 2599-2626, 2024.
Chu, D., Wan, B., Liu, Y., Li, L., Li, H., Fang, F., Li, S., Pan, S., and Wang, M.: An integrated machine learning framework using borehole descriptions for 3D lithological modeling, Engineering Geology, 351, 108050, 2025.
de la Varga, M., Schaaf, A., and Wellmann, F.: GemPy 1.0: open-source stochastic geological modeling and inversion, Geoscientific Model Development, 12, 1-32, 10.5194/gmd-12-1-2019, 2019.
Du, L., Du, J., Fang, Z., Shah, S. Y. A., Kablan, O. A. B. K., Zhang, B., and Tan, J.: A Recurrent Neural Network Surrogate Model with Few-Shot Strategy for CO2 Storage in Deep Subsurface Saline Aquifer with Limited Direct Numerical Simulation Samples, Lithosphere, 2026, 10.2113/lithosphere_2025_139, 2026.
Fang, Z. and Zhang, B.: Three-Dimensional Geological Modeling based on Dual-Task Stratigraphy-Aware Attention Networks (Geo-SAN v1.0), Zenodo [dataset], 10.5281/zenodo.19903694, 2026.
Fey, M. and Lenssen, J. E.: Fast Graph Representation Learning with PyTorch Geometric, arXiv, 1903.02428, 2019.
Gao, K. and Wellmann, F.: Fault representation in structural modelling with implicit neural representations, Computers & Geosciences, 199, 105911, https://doi.org/10.1016/j.cageo.2025.105911, 2025.
Giraud, J., Caumon, G., Grose, L., Ogarko, V., and Cupillard, P.: Integration of automatic implicit geological modelling in deterministic geophysical inversion, Solid Earth, 15, 63-89, 10.5194/se-15-63-2024, 2024.
Gori, M., Monfardini, G., and Scarselli, F.: A new model for learning in graph domains, Proceedings. 2005 IEEE International Joint Conference on Neural Networks, 2005., 31 July-4 Aug. 2005, 10.1109/IJCNN.2005.1555942, 2005.
Guo, J., Xu, X., Wang, L., Wang, X., Wu, L., Jessell, M., Ogarko, V., Liu, Z., and Zheng, Y.: GeoPDNN 1.0: a semi-supervised deep learning neural network using pseudo-labels for three-dimensional shallow strata modelling and uncertainty analysis in urban areas from borehole data, Geosci. Model Dev., 17, 957-973, 10.5194/gmd-17-957-2024, 2024.
Guo, J., Wang, J., Wu, L., Liu, C., Li, C., Li, F., Lin, M., Jessell, M. W., Li, P., Dai, X., and Tang, J.: Explicit-implicit-integrated 3-D geological modelling approach: A case study of the Xianyan Demolition Volcano (Fujian, China), Tectonophysics, 795, 10.1016/j.tecto.2020.228648, 2020.
Hamilton, W., Ying, Z., and Leskovec, J.: Inductive representation learning on large graphs, Advances in neural information processing systems, 30, 2017.
He, Z., Xu, X., Peng, P., Wang, L., and Tian, S.: A deep learning-driven three-dimensional geological modeling method using sparse borehole sampling data, Measurement, 118461, 2025.
Hillier, M., de Kemp, E., and Schetselaar, E.: 3D form line construction by structural field interpolation (SFI) of geologic strike and dip observations, Journal of Structural Geology, 51, 167-179, 10.1016/j.jsg.2013.01.012, 2013.
Hillier, M., Wellmann, F., Brodaric, B., de Kemp, E., and Schetselaar, E.: Three-Dimensional Structural Geological Modeling Using Graph Neural Networks, Mathematical Geosciences, 53,

https://doi.org/10.5194/egusphere-2026-1210
Preprint. Discussion started: 18 May 2026

1725-1749, 10.1007/s11004-021-09945-x, 2021.
Hillier, M., Wellmann, F., de Kemp, E. A., Brodaric, B., Schetselaar, E., and Bédard, K.: GeoINR 1.0: an implicit neural network approach to three-dimensional geological modelling, Geosci. Model Dev., 16, 6987-7012, 10.5194/gmd-16-6987-2023, 2023.
Hu, Y., Wang, Z. Z., Guo, X., Kek, H. Y., Ku, T., Goh, S. H., Leung, C. F., Tan, E., and Zhang, Y.: Three-dimensional reconstruction of subsurface stratigraphy using machine learning with neighborhood aggregation, Engineering Geology, 337, 107588, 2024.
Jessell, M., Guo, J., Li, Y., Lindsay, M., Scalzo, R., Giraud, J., Pirot, G., Cripps, E., and Ogarko, V.: Into the Noddyverse: a massive data store of 3D geological models for machine learning and inversion applications, Earth System Science Data, 14, 381-392, 10.5194/essd-14-381-2022, 2022.
Khan, M. S., Kim, I. S., and Seo, J.: A boundary and voxel-based 3D geological data management system leveraging BIM and GIS, International Journal of Applied Earth Observation and Geoinformation, 118, 103277, https://doi.org/10.1016/j.jag.2023.103277, 2023.
Khan, U., Zhang, B., Du, J., and Jiang, Z.: 3D structural modeling integrated with seismic attribute and petrophysical evaluation for hydrocarbon prospecting at the Dhulian Oilfield, Pakistan, Front. Earth Sci., 15, 649-675, 10.1007/s11707-021-0881-1, 2021.
Li, C., Li, F., Liu, C., Tang, Z., Fu, S., Lin, M., Lv, X., Liu, S., and Liu, Y.: Deep learning-based geological map generation using geological routes, Remote Sensing of Environment, 309, 114214, 2024.
Lyu, B., Wang, Y., and Shi, C.: Multi-scale generative adversarial networks (GAN) for generation of three-dimensional subsurface geological models from limited boreholes and prior geological knowledge, Computers and Geotechnics, 170, 106336, 2024.
Peng, J.-Z., Hua, Y., Aubry, N., Chen, Z.-H., Mei, M., and Wu, W.-T.: Data and physics-driven modeling for fluid flow with a physics-informed graph convolutional neural network, Ocean Engineering, 301, 117551, https://doi.org/10.1016/j.oceaneng.2024.117551, 2024.
Reichstein, M., Camps-Valls, G., Stevens, B., Jung, M., Denzler, J., Carvalhais, N., and Prabhat, F.: Deep learning and process understanding for data-driven Earth system science, Nature, 566, 195-204, 2019.
Ren, A., Wu, L., Xu, J., Xing, Y., Qiu, Q., and Xie, Z.: A deep learning method for 3D geological modeling using ET4DD with offset-attention mechanism, Computers & Geosciences, 200, 105929, 2025.
Shah, S. Y. A., Du, J., Iqbal, S. M., Du, L., Khan, U., Zhang, B., and Tan, J.: Integrated Three-Dimensional Structural and Petrophysical Modeling for Assessment of CO2 Storage Potential in Gas Reservoir, Lithosphere, 2024, 10.2113/2024/lithosphere_2024_222, 2024.
Sprague, K. B. and De Kemp, E. A.: Interpretive tools for 3-D structural geological modelling part II: Surface design from sparse spatial data, GeoInformatica, 9, 5-32, 2005.
Veličković, P., Cucurull, G., Casanova, A., Romero, A., Lio, P., and Bengio, Y.: Graph attention networks, arXiv preprint arXiv:1710.10903, 2017.
Wang, G., Zhu, Y., Zhang, S., Yan, C., Song, Y., Ma, Z., Hong, D., and Chen, T.: 3D geological modeling based on gravitational and magnetic data inversion in the Luanchuan ore region, Henan Province, China, Journal of Applied Geophysics, 80, 1-11, 10.1016/j.jappgeo.2012.01.006, 2012.
Wang, L., Jiang, Z., Song, L., Yu, X., Yuan, S., and Zhang, B.: A groundwater level spatiotemporal prediction model based on graph convolutional networks with a long short-term memory, Journal of Hydroinformatics, 26, 2962-2979, 10.2166/hydro.2024.226, 2024.
Wang, L., Yin, Y., Zhang, C., Feng, W., Li, G., Chen, Q., and Chen, M.: A MPS-based novel method

https://doi.org/10.5194/egusphere-2026-1210
Preprint. Discussion started: 18 May 2026

of reconstructing 3D reservoir models from 2D images using seismic constraints, Journal of Petroleum Science and Engineering, 209, 10.1016/j.petrol.2021.109974, 2022.

Wang, L. F., Wu, X. B., Zhang, B. Y., Li, X. F., Huang, A. S., Meng, F., and Dai, P. Y.: Recognition of Significant Surface Soil Geochemical Anomalies Via Weighted 3D Shortest-Distance Field of Subsurface Orebodies: A Case Study in the Hongtoushan Copper Mine, NE China, Natural Resources Research, 28, 587-607, 10.1007/s11053-018-9410-7, 2019.

Wellmann, J. F., de la Varga, M., Murdie, R. E., Gessner, K., and Jessell, M.: Uncertainty estimation for a geological model of the Sandstone greenstone belt, Western Australia - insights from integrated geological and geophysical inversion in a Bayesian inference framework, in: Characterization of Ore-Forming Systems from Geological, Geochemical and Geophysical Studies, edited by: Gessner, K., Blenkinsop, T. G., and Sorjonen-Ward, P., Geological Society of London, London, 453-464, https://doi.org/10.6084/m9.figshare.c.3899719.v1, 2017.

Yin, L., Guo, Y., Wang, L., Yuan, S., Fang, Z., and Zhang, B.: A Dual-Transformer Network for Spatiotemporal Modeling of Carbon Dioxide Column Concentration (XCO2) on the Basis of Dynamic Heterogeneous Graphs, Transactions in GIS, 30, e70275, https://doi.org/10.1111/tgis.70275, 2026.

Zhang, B., Du, L., Khan, U., Tong, Y., Wang, L., and Deng, H.: AdaHRBF v1.0: gradient-adaptive Hermite–Birkhoff radial basis function interpolants for three-dimensional stratigraphic implicit modeling, Geosci. Model Dev., 16, 3651-3674, 10.5194/gmd-16-3651-2023, 2023a.

Zhang, B., Li, M., Huan, Y., Khan, U., Wang, L., and Wang, F.: Bedrock mapping based on terrain weighted directed graph convolutional network using stream sediment geochemical samplings, Transactions of Nonferrous Metals Society of China, 33, 2799-2814, 2023b.

Zhang, B., Xu, Z., Wei, X., Song, L., Shah, S. Y. A., Khan, U., Du, L., and Li, X.: Deep Subsurface Pseudo-Lithostratigraphic Modeling Based on Three-Dimensional Convolutional Neural Network (3D CNN) Using Inversed Geophysical Properties and Shallow Subsurface Geological Model, Lithosphere, 2024, 10.2113/2024/lithosphere_2023_273, 2024.